Crystallinity, exchange-correlation and isotope effects on the plasmon excitations in high T_c superconductors

1992 J. Phys.: Condens. Matter 4 3533

(http://iopscience.iop.org/0953-8984/4/13/016)

J. Phys.: Condens. Matter 4 (1992) 3533–3550. Printed in the UK

Crystallinity, exchange–correlation and isotope effects on the plasmon excitations in high-T_c superconductors

Danhong Huang†, Chao Zhang‡ and Godfrey Gumbs†§

† Department of Physics, University of Lethbridge, Lethbridge, Alberta T1K 3M4, Canada
‡ TRIUMF, 4004 Wesbrook Mall, Vancouver, B.C. V6T 2A3, Canada
§ Department of Physics and Astronomy, Hunter College of the City University of New York, 695 Park Avenue, New York, NY 10021, USA

Abstract. With the use of a tight-binding model we have studied the effects due to crystallinity, i.e. the atomic structure, of the $Cu–O_2$ planes and Cu–O chain planes of the high-T_c superconductors on the intralayer and interlayer Coulomb interactions as well as the density–density response function. This effect is found to be appreciable since each electron is well localized around the copper site and the size of the unit cell is comparable with the lattice constant. Localization leads to poor conductivity in the normal state and is determined by the hopping between adjacent copper sites caused by the overlap of electron wavefunctions with electrons on the oxygen site. The dominant local exchange–correlation contribution is included in the local-field approximation. By taking account of the plasmon–optical phonon coupling in our calculations, we have demonstrated the isotope effect for acoustical plasmon-mediated pairing as well as the effect on the effective intralayer Coulomb interaction which is believed to be important for the formation of Cooper pairs in the $Cu–O_2$ planes. The effects due to the position of the chain planes and the number of planes in each unit cell on the plasmon excitation energies as well as the effective intralayer Coulomb interaction are also studied. The relationship between these effects and the critical temperature T_c is discussed.

1. Introduction

The recent discovery of high-T_c superconductors has stimulated a remarkable surge of interest and extensive discussions on the mechanisms responsible for superconductivity [1–4]. In view of the reduced or negligible isotope effect [5] in layered high-T_c superconductors and the fact that phonons are not likely to account for transition temperatures in excess of 40–50 K, we are now searching for other types of mechanisms which might be responsible. Included among the alternative mechanisms is the role played by acoustical plasmons [6–8]. Several experiments have demonstrated that the conductivity is isotropic within the plane and is greatly reduced in the direction perpendicular to the planes. This implies that the layered two-dimensional (2D) electron gas (EG) planes are most likely to be responsible for the superconductivity of these materials. The common feature of these materials is the layered 2D planar structure in which the planes are coupled to each other by the interlayer Coulomb interaction. This gives rise to a singular behaviour for the plasmon density of states at the Brillouin zone boundaries [7], which in turn leads to a noticeable contribution to the acoustical plasmon-mediated pairings.

Most of the theoretical work that has been carried out so far on this problem has been restricted to models consisting of a superlattice of homogeneous 2D EG layers

0953-8984/92/133533+18$04.50

[6–10]. In this paper, we include the effect due to crystallinity and we discuss the main difference and physical consequences which this inclusion has on the collective modes of high-temperature superconductors. There are several features in our results which are due to the inclusion of the crystalline structure in our model. (To define the notation, we show the structure of $YBa_2Cu_3O_7$ in figure 1.) For example, the inclusion of crystallinity produces a local minimum in the excitation energy at the Brillouin zone boundary due to the competition between the increase in polarization and the decrease in the Coulomb interaction. This causes the plasmon cut-off frequency to be shifted downwards. Within the tight-binding model, this causes the excitation energy to depend on the position of the chain planes. Both the single-particle and plasmon excitation energies are periodic in the wavevector components q_x and q_y with period $2\pi/a$, where a is the period shown in figure 1. Also, since the conductivity is poor in the normal state of these materials and the size of the unit cell is comparable with the lattice constant, we believe that the crystalline structure produces important modifications of the intralayer and interlayer Coulomb interactions as well as the density–density response function.

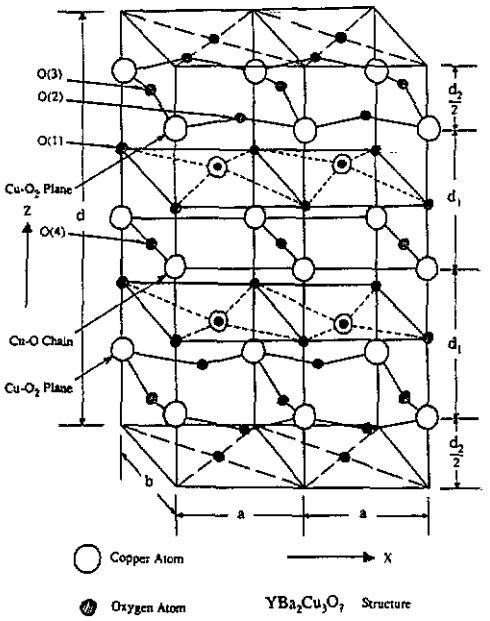

Figure 1. Schematic representation of the crystal structure of $YBa_2Cu_3O_7$. The Cu–O_2 plane and Cu–O chain plane are indicated. The oxygen atoms O(2), O(3) and O(4) give rise to hopping between adjacent copper sites. Here, $d_1' = d_1'' = d_1$ and the length of the unit cell along the z-axis is $d = 2d_1 + d_2$. d_1', (d_1'') are the separations between the chain plane and the adjacent upper (lower) plane. The Cu–O chain is parallel to the y-axis and the Cu–O_2 plane is in the x–y plane, with lattice constants a, b in the x- and y-directions, respectively.

From bandstructure calculations, we know that the active electrons are well localized around the copper sites. The presence of oxygen atoms produces an indirect hopping of the electrons between adjacent copper sites as a result of the overlap of the electron wavefunctions with electrons on the oxygen sites. This implies a poor hopping conductivity within a plane in the normal state. This is also the case

for the chains in figure 1. At half-filling, the undoped materials are Mott insulators. After doping with holes, the lowest electron energy band is no longer completely filled. The intraband transition for electrons is then allowed. We only consider the dynamics of the electrons. Hole doping is included to account for the incompletely filled lowest energy band. Since we are only interested in charge density oscillations, we shall neglect the spin–spin Heisenberg exchange interaction. When the correlations are strong, the random phase approximation (RPA) is not suitable. In this limit, we must include effects due to local exchange and correlations which modify the short-ranged part of the intralayer Coulomb interaction. The role played by the chain planes is to increase the coupling between pairs of unit cells. This also leads to an anisotropic sound velocity of acoustical plasmons within a plane. Contrary to expectation, the chain excitations do not increase the weight of acoustical plasmons in the density of states as a result of the large effective mass and the Landau damping of single-particle excitations within a plane. When we assume that the pairing is due to acoustical plasmon-mediated pairing, we show that there exists a weak isotope effect, in the sense that the mass of an oxygen ion includes contributions to the shifts to the optical phonon frequency and plasmon cut-off frequency when the coupling between plasmons and phonons is included. The aim of our paper is to generalize the well-known homogeneous EG model for plasmon excitations in high-T_c superconductors to include the inhomogeneity of the electronic structure within the planes. We simulate the layered inhomogeneous EG by a planar array of quantum dots. We include the tunnelling between adjacent dots in both the x- and y-directions within a plane as the model for the Cu–O_2 plane. As a model for the Cu–O chain plane, we include tunnelling only along the y-direction (the chain direction).

For simplicity, we choose the single-particle confining potential of the copper atoms within a plane and on a chain to be of parabolic form

$$\frac{1}{2}m^*_{p(c)}\left(\frac{U_{p(c)}}{\hbar}\right)^2(x^2+y^2)$$

where $m^*_{p(c)}$ is the effective mass of an electron in the plane (chain), and $U_{p(c)}$ are the strengths of the confining potential for the plane (chain). The oxygen atoms O(2), O(3) and O(4) also produce indirect hopping between adjacent copper sites with intensity $t_p = t_x = t_y$ within a plane and $t_c = t_y$ along a chain. The bandwidths are $W_p = 4t_p$ ($W_c = 4t_c$) in the plane (and on a chain). The thickness of the Cu–O_2 planes and the Cu–O chain planes is taken to be L_z. The width of the chain is much smaller than the lattice constant.

This paper is arranged as follows. In section 2, we present our model which takes account of the crystalline structure of high-T_c superconductors, local exchange–correlation effects as well as plasmon–phonon coupling. In section 3, we present numerical results and a discussion. In section 4, we discuss the connection between our results and high-T_c superconductivity.

2. Model and general formalism

In the tight-binding approximation, the first-order single-particle energy eigenvalues and eigenfunctions have been calculated for a single layer of multiple chains as [11]

$$E^{(c)}_{ij}(k_y) = E^{(c)}_{ij} + \frac{W_c}{2}(1-\cos(k_y a)) \tag{1}$$

$$|k_x, k_y; i, j >= \eta(z) \sum_{n,m} \frac{1}{\sqrt{N_x N_y}} \exp(ik_x na + ik_y ma) \xi_i(x - na) \gamma_j(y - ma) \tag{2}$$

where W_c is the bandwidth for tunnelling motion in the y-direction parallel to the chains. Here, $n, m = 0, \pm 1, \pm 2, \ldots$ are the indices along the x- and y-directions, and $i, j = 0, 1, 2, \ldots$ are the level indices for the lateral quantization. N_x, N_y are normalization factors for the periodic boundary conditions imposed. Here, the first summation over m in (2) is for the Bloch wavefunction of a single chain, and the second summation over n is for the array of chains. $\eta(z)$ is a variational wavefunction [11], representing the confinement in the z-direction, and is given by

$$\eta(z) = \begin{cases} \frac{z}{\sqrt{2L_z^3}} \exp\left(-\frac{z}{2L_z}\right) & \text{for } z \geqslant 0 \\ 0 & \text{for } z < 0 \end{cases} \tag{3}$$

where L_z is the thickness of the layer. In our model, the z-dependent part of the wavefunction in (3) is included to account for the small correction to the screening given by (19) due to the finite thickness L_z of the layer. We may also use the wavefunction for a square-well model with infinite potential barriers to simulate the boundaries. However, for the case considered here, i.e. $q_{xy} L_z \ll 1$ (thin film limit), the different forms of model wavefunctions only give very small differences in the screening factor $I(q_{xy} L_z)$ in (19) which is approximately equal to one in the thin film limit. Since the z-dependent part of the wavefunction decays very rapidly with distance from the centre of plane due to the very narrow region of confinement, the variation of $I(q_{xy} L_z)$ from a value of unity is quite small. The wavefunction in (3) has been chosen to simplify the mathematical details of our calculations. The wavefunctions $\xi_i(x-na)$ and $\gamma_j(y-ma)$ depend on the model confining potentials in the x- and y-directions. When the single-particle harmonic confining potential model is used, $\xi_i(x-na)$ and $\gamma_j(y-ma)$ are the usual harmonic oscillator wavefunctions.

For a single-layer of planar 2D EG, the electronic wavefunctions are still given by (2) to first order. The corresponding single-particle energy eigenvalues are [11]

$$E_{ij}^{(p)}(k_x, k_y) = E_{ij}^{(p)} + \frac{W_p}{2}(1 - \cos(k_x a)) + \frac{W_p}{2}(1 - \cos(k_y a)) \tag{4}$$

where W_p is the bandwidth due to nearest-neighbour hopping. For both the chain and plane, we have assumed that the electrons are always in the lowest eigenstate as a result of the very strong confinement in the z-direction. Also, we have neglected the very small anisotropy in the lattice constants along the x- and y-directions, and denoted their average value by a. Since only the lowest electronic states are occupied and since we are only interested in the low-energy intraband excitations, we can set $i = j = 0$ in equations (1) and (4). In the weak tunnelling limit, the irreducible polarizabilities of the chain and plane have been calculated and the results for the real parts are [11]

$$\text{Re } \chi_0^{(c)}(q_y, \omega) = \frac{2W_c n_{1D}}{a\hbar^2\omega^2} \left[\frac{\sin(k_{yF} a)}{k_{yF} a}\right] \sin^2\left(\frac{q_y a}{2}\right) \tag{5}$$

$$\text{Re } \chi_0^{(p)}(q_x, q_y, \omega) = \frac{2W_p \bar{n}_s}{\hbar^2\omega^2} \left[\frac{\sin(k_F a)}{k_F a}\right]^2 \left[\sin^2\left(\frac{q_x a}{2}\right) + \sin^2\left(\frac{q_y a}{2}\right)\right] \tag{6}$$

where $\bar{n}_s$ and n_{1D} are the areal and linear electron densities in the plane and chain, respectively. k_{yF} and k_F are the Fermi wavevectors of the chain and plane and are given by

$$k_{yF} = \pi n_{1D} \tag{7}$$

$$k_F = \pi(\bar{n}_s)^{1/2}. \tag{8}$$

We are only interested in the regime where there is no Landau damping, i.e. when $q < 2k_{yF}^{(c)}$. Here, $k_{yF}^{(c)}$ is the Fermi wavevector for the chains. Also, in this region, we have $\omega \gg q$. Therefore, we use the long-wavelength approximation for the susceptibility in equations (5) and (6), and neglect the instabilities that are produced at $q = 2k_{yF}^{(c)}$ where the modes are Landau damped. The imaginary parts of the polarizabilities account for Landau damping in the region $\omega_{min} < \omega < \omega_{max}$. For the chain, we have

$$\hbar\omega_{min}^{(c)} = \begin{cases} \left(W_c - 2\epsilon_F^{(c)}\right)\sin^2\left(\frac{q_y a}{2}\right) - \sqrt{\epsilon_F^{(c)}\left(W_c - \epsilon_F^{(c)}\right)}\,|\sin(q_y a)| & q_y \geqslant q_c \\ \sqrt{\epsilon_F^{(c)}\left(W_c - \epsilon_F^{(c)}\right)}\,|\sin(q_y a)| - \left(W_c - 2\epsilon_F^{(c)}\right)\sin^2\left(\frac{q_y a}{2}\right) & q_y < q_c \end{cases} \tag{9}$$

and

$$\hbar\omega_{max}^{(c)} = \left(W_c - 2\epsilon_F^{(c)}\right)\sin^2\left(\frac{q_y a}{2}\right) + \sqrt{\epsilon_F^{(c)}\left(W_c - \epsilon_F^{(c)}\right)}\,|\sin(q_y a)| \tag{10}$$

where the threshold wavevector and the Fermi energy are

$$q_c = \frac{2}{a}\tan^{-1}\left[\frac{2\sqrt{\epsilon_F^{(c)}\left(W_c - \epsilon_F^{(c)}\right)}}{W_c - 2\epsilon_F^{(c)}}\right] \tag{11}$$

$$\epsilon_F^{(c)} = W_c \sin^2\left(\frac{\pi}{2} n_{1D} a\right). \tag{12}$$

Similarly, for the plane, when $q_x = 0$, we obtain

$$\hbar\omega_{min}^{(p)} = \begin{cases} \left(W_p - 2\epsilon_F^{(p)}\right)\sin^2\left(\frac{q_y a}{2}\right) - \sqrt{\epsilon_F^{(p)}\left(W_p - \epsilon_F^{(p)}\right)}\,|\sin(q_y a)| & q_y \geqslant q_p \\ 0 & q_y < q_p \end{cases} \tag{13}$$

and

$$\hbar\omega_{max}^{(p)} = \begin{cases} W_p\,|\sin\tfrac{1}{2}(q_y a)| & q_y \geqslant \frac{\pi}{a} - q_p \\ \left(W_p - 2\epsilon_F^{(p)}\right)\sin^2\tfrac{1}{2}(q_y a) + \sqrt{\epsilon_F^{(p)}\left(W_p - \epsilon_F^{(p)}\right)}\,|\sin(q_y a)| & q_y < \frac{\pi}{a} - q_p \end{cases} \tag{14}$$

where the threshold wavevector and the Fermi energy are

$$q_{\mathrm{p}} = \frac{2}{a}\sin^{-1}\left[\frac{2\sqrt{\epsilon_{\mathrm{F}}^{(\mathrm{p})}\left(W_{\mathrm{p}} - \epsilon_{\mathrm{F}}^{(\mathrm{p})}\right)}}{W_{\mathrm{p}}}\right] \tag{15}$$

$$\epsilon_{\mathrm{F}}^{(\mathrm{p})} = W_{\mathrm{p}}\sin^2\left(\frac{\pi}{2}\left(\bar{n}_s a^2\right)^{1/2}\right). \tag{16}$$

When $q_y = 0$, we can replace q_y in equations (13) and (14) by q_x. In equations (9)–(11), we have assumed that $W_{\mathrm{c}} \geqslant 2\epsilon_{\mathrm{F}}^{(\mathrm{c})}$ and $W_{\mathrm{p}} \geqslant 2\epsilon_{\mathrm{F}}^{(\mathrm{p})}$ which are satisfied when $n_{1\mathrm{D}}a \leqslant \frac{1}{2}$ and $\bar{n}_s a^2 \leqslant \frac{1}{4}$. We note that the bandwidth is proportional to the reciprocal of the effective mass and for simplicity we take $U_{\mathrm{c}}/t_{\mathrm{c}} = U_{\mathrm{p}}/t_{\mathrm{p}}$. As a result, we have $m_{\mathrm{c}}^* U_{\mathrm{c}} = m_{\mathrm{p}}^* U_{\mathrm{p}} = m^* U$. For these assumptions, both the chain and the plane have the same form of intralayer Coulomb interaction [11]

$$D_0\left(q_x, q_y\right) = \frac{2\pi e^2}{\varepsilon_s}\sum_{n,m}\frac{I\left(q_{nm}L_z\right)}{q_{nm}}\exp\left(-\frac{\hbar^2 q_{nm}^2}{2m^* U}\right) \tag{17}$$

$$q_{nm} = \left[\left(q_x + nG\right)^2 + \left(q_y + mG\right)^2\right]^{1/2} \tag{18}$$

$$I\left(q_{nm}L_z\right) = \frac{\left(8 + 9q_{nm}L_z + 3q_{nm}^2 L_z^2\right)}{8\left(1 + q_{nm}L_z\right)^3}. \tag{19}$$

Here, $G = 2\pi/a$ is a reciprocal lattice vector. The interlayer Coulomb interaction can be calculated in a similar way with the result

$$D_1\left(q_x, q_y; s\right) = \frac{2\pi e^2}{\varepsilon_s}\sum_{n,m}\frac{I\left(q_{nm}L_z\right)}{q_{nm}}\exp\left(-\frac{\hbar^2 q_{nm}^2}{2m^* U}\right)\exp\left(-q_{nm}s\right) \tag{20}$$

where s is the separation between adjacent layers. In equations (17) and (20), the medium surrounding the system has dielectric constant $\varepsilon_s = 4\pi\varepsilon_0\varepsilon_r$.

We include effects due to exchange and correlation in the local-field approximation [9]. The renormalized polarizability is given by

$$\chi_{\mathrm{eff}}^{(\mathrm{p}),(\mathrm{c})}\left(q_x, q_y; \omega\right) = \frac{\chi_0^{(\mathrm{p}),(\mathrm{c})}\left(q_x, q_y; \omega\right)}{1 + G^{(\mathrm{p}),(\mathrm{c})}\left(q_x, q_y\right) D_0\left(q_x, q_y\right)\chi_0^{(\mathrm{p}),(\mathrm{c})}\left(q_x, q_y; \omega\right)} \tag{21}$$

where the local-field correction is accounted for by the factor

$$G^{(\mathrm{p})}\left(q_x, q_y\right) = \frac{q_{xy}}{\left[\left(2q_{xy}\right)^2 + \left(\pi k_{\mathrm{F}}\right)^2\right]^{1/2}} \tag{22}$$

and $G^{(\mathrm{c})}\left(q_x, q_y\right)$ is obtained by replacing k_{F} by $k_{y\mathrm{F}}$ in (22) [9]. The local-field correction in (22) has the same form as in [9]. It includes a correction to the RPA

due to the short-range part of the electron–electron interaction. Furthermore, we incorporate the plasmon–phonon coupling into our formalism through

$$\bar{\chi}_{\rm eff}^{({\rm p}),({\rm c})}(q_x,q_y;\omega)=\left[1+\left(1-\frac{\varepsilon_\infty}{\varepsilon_{\rm st}}\right)\frac{\omega_{\rm LO}^{({\rm p}),({\rm c})2}}{\omega^2-\omega_{\rm LO}^{({\rm p}),({\rm c})2}}\right]\chi_{\rm eff}^{({\rm p}),({\rm c})}(q_x,q_y;\omega) \tag{23}$$

where ε_∞ and $\varepsilon_{\rm st}$ are the optical and static background dielectric constants of the material and $\omega_{\rm LO}^{({\rm p})}$, $\omega_{\rm LO}^{({\rm c})}$ are the optical phonon frequencies of the plane and chain, respectively.

We note that there is an exponentially decaying factor in the interlayer Coulomb interaction in (20). To simplify the calculation, we use the tight-binding model [10] to calculate the excitation energy. In this approximation, the excitation energy is a solution of the secular equation

$$\det\ \underline{\varepsilon}(q_x,q_y;\omega)=\begin{vmatrix}\cdots&\cdots&\cdots&\cdots&\cdots&\cdots&\cdots&\cdots&\cdots\\ \cdots&E&A&B&0&\cdots&0&0&\cdots\\ \cdots&0&B&A&E&\cdots&0&0&\cdots\\ \cdots&0&0&D&C&D&0&0&\cdots\\ \cdots&0&0&0&E&A&B&0&\cdots\\ \cdots&0&0&0&0&B&A&E&\cdots\\ \cdots&0&0&0&0&0&D&C&D\\ \cdots&0&0&0&0&0&0&E&A\\ \cdots&\cdots&\cdots&\cdots&\cdots&\cdots&\cdots&\cdots&\cdots\end{vmatrix}=0 \tag{24}$$

where

$$A=1-\bar{\chi}_{\rm eff}^{({\rm p})}(q_x,q_y;\omega)\,D_0(q_x,q_y) \tag{25}$$

$$B(d_2)=-\bar{\chi}_{\rm eff}^{({\rm p})}(q_x,q_y;\omega)\,D_1(q_x,q_y;d_2) \tag{26}$$

$$C=1-\bar{\chi}_{\rm eff}^{({\rm c})}(q_x,q_y;\omega)\,D_0(q_x,q_y) \tag{27}$$

$$D(d_1')=-\bar{\chi}_{\rm eff}^{({\rm c})}(q_x,q_y;\omega)\,D_1(q_x,q_y;d_1') \tag{28}$$

$$E(d_1'')=-\bar{\chi}_{\rm eff}^{({\rm p})}(q_x,q_y;\omega)\,D_1(q_x,q_y;d_1'') \tag{29}$$

and d_1', (d_1'') are the separations between the chain plane and the adjacent upper (lower) plane. The length of the unit cell along the z-direction is $d=(d_2+d_1'+d_1'')$. As discussed in [10], the areal and linear electron densities are related to the three-dimensional (3D) electron density through

$$\bar{n}_{\rm s}=n_{\rm 3D}d_2 \tag{30}$$

$$n_{\rm 1D}=n_{\rm 3D}a\,(d_1'+d_1''-d_2)\,. \tag{31}$$

From a dynamical point of view, the structure must be 3D. Otherwise, thermal fluctuations will destroy any long-range order in the thermodynamic limit. Electrically, the system can be regarded as 2D due to the appreciable anisotropy in the conductivity. As in the layered homogeneous 2D EG model previously discussed in

the literature [8, 9], we have neglected the wavefunction overlap along the direction perpendicular to the plane (one order smaller than within the plane). It is known that this wavefunction overlap only leads to a negligible gap (much smaller that $k_B T$) in the excitation spectrum as well as a very small modification to the screening. In principle, if a plasmon-mediated mechanism is assumed, we could calculate the transition temperature T_c from the gap equation. The effective intralayer Coulomb interaction plays a dominant role in this equation. In conventional Bardeen–Cooper–Schrieffer (BCS) theory, it is the pair potential that is included. Here, the effective intralayer Coulomb interaction can be calculated as follows. A simplifying assumption is to take a unit cell that contains one $Cu–O_2$ layer and one Cu–O chain layer. For this, we obtain

$$U_{\text{eff}}(q;\omega) = \frac{V_{\text{p}}(q)\epsilon_{\text{c}}(q) + |\bar{V}(q)|^2 \chi_0^{(\text{c})}(q_y,\omega)}{\epsilon(q;\omega)} \tag{32}$$

where $q = (q_x, q_y, q_z)$ and

$$V_{p,(\text{c})}(q) = \left[1 + \left(1 - \frac{\varepsilon_\infty}{\varepsilon_{\text{st}}}\right) \frac{\omega_{\text{LO}}^{(\text{p}),(\text{c})2}}{\omega^2 - \omega_{\text{LO}}^{(\text{p}),(\text{c})2}} \frac{1}{(1 + q_z^2 L_z^2)^3}\right] \times \left[F_1(q) - G^{(\text{p}),(\text{c})}(q) D_0(q)\right] \tag{33}$$

with

$$F_1(q) = \frac{2\pi e^2}{\varepsilon_{\text{s}}} \sum_{n,m} \frac{I(q_{nm} L_z)}{q_{nm}} \exp\left(-\frac{\hbar^2 q_{nm}^2}{2m^* U}\right) \frac{\sinh(q_{nm} d)}{\cosh(q_{mn} d) - \cos(q_z d)}. \tag{34}$$

In (32), we have introduced $\epsilon(q;\omega)$ which is defined by

$$\epsilon(q;\omega) = \epsilon_{\text{p}}(q;\omega)\epsilon_{\text{c}}(q;\omega) - |\bar{V}(q)|^2 \chi_0^{(\text{p})}(q_x, q_y;\omega)\, \chi_0^{(\text{c})}(q_y;\omega) \tag{35}$$

where the interlayer coupling potential $\bar{V}(q)$ is given by

$$|\bar{V}(q)|^2 = \left[1 + \left(1 - \frac{\varepsilon_\infty}{\varepsilon_{\text{st}}}\right) \frac{\omega_{\text{LO}}^{(\text{c})2}}{\omega^2 - \omega_{\text{LO}}^{(\text{c})2}} \frac{1}{(1 + q_z^2 L_z^2)^3}\right] \times \left[1 + \left(1 - \frac{\varepsilon_\infty}{\varepsilon_{\text{st}}}\right) \frac{\omega_{\text{LO}}^{(\text{p})2}}{\omega^2 - \omega_{\text{LO}}^{(\text{p})2}} \frac{1}{(1 + q_z^2 L_z^2)^3}\right] \times \left| \frac{2\pi e^2}{\varepsilon_{\text{s}}} \sum_{n,m} \frac{I(q_{nm} L_z)}{q_{nm}} \exp\left(-\frac{\hbar^2 q_{nm}^2}{2m^* U}\right) \times \frac{\sinh(q_{nm}(d - d_1')) + e^{-iq_z d} \sinh(q_{nm} d_1')}{\cosh(q_{mn} d) - \cos(q_z d)} e^{iq_z d_1'} \right|^2 \tag{36}$$

and

$$\epsilon_{\text{p(c)}}(q;\omega) = 1 - V_{\text{p(c)}}(q) \chi_0^{(\text{p}),(\text{c})}(q;\omega) \tag{37}$$

where d_1' is the separation between the chain plane and the adjacent upper plane. In comparison, the effective potential for a layered 2D EG is

$$U_{\text{eff}}(q;\omega) = \frac{(2\pi e^2/\varepsilon_{\text{s}} q_{xy}) \sinh(q_{xy} d)}{\cosh(q_{xy} d) - \cos(q_z d) - (2\pi e^2 \bar{n}_{\text{s}} q_{xy}/\varepsilon_{\text{s}} m_{\text{p}}^* \omega^2) \sinh(q_{xy} d)}. \tag{38}$$

By computing the ratio of (32) to (38) we could determine the effect due to crystallinity, exchange and correlation as well as plasmon–phonon coupling on the effective intralayer Coulomb interaction.

3. Numerical results

We take the following material parameters from [10] and use them in our calculations:

$$n_{3D} = 4.0 \times 10^{21}\ \mathrm{cm}^{-3} \qquad m_c^* = 6.20\ m_e \qquad m_p^* = 1.43\ m_e \qquad a = 3.85\ \text{Å}$$

$$d_1 = 4.13\ \text{Å} \qquad d_2 = 3.42\ \text{Å} \qquad L_z = 2a_B^* = 0.68\ \text{Å}$$

$$\varepsilon_r = \varepsilon_\infty = 4.0 \qquad \varepsilon_{st} = 12.0.$$

The bandwidths W_p and W_c have not played a role in previous theories. We take $W_p = 1.0$ eV for which we have $\epsilon_F^{(p)} = 0.42$ eV which compares well with the value used in [10]. Since $W_c/W_p \approx m_p^*/m_c^*$ we obtain $W_c = 0.23$ eV. For the quantum dot model, the strength of the confining potential U for each dot and the tunnelling intensity t between adjacent dots are two parameters in our model. In our numerical calculations, we took t to be the hopping parameter in the Hubbard model. We note that if we assume a parabolic confining potential, the magnitude of the gap between the lowest and the first excited levels is a measure of the strength of the confining potential. Also, in our calculations, we have chosen the value for U to be the same as the Hubbard interaction parameter. However, we emphasize that our work is not related to the Hubbard model. We have simply used the values of the parameters in the Hubbard model to carry out the numerical calculations in our paper. Our calculations show that our results are sensitive only to the bandwidth W but not U. The calculation [12] of normal state properties has shown that the best fitting to experimental data could be obtained when $U/W = 3$. We make use of this result and obtain $U_p = 3.0$ eV and $U_c = 0.69$ eV. Also, from experiment [13], we get for O_{16}

$$\hbar\omega_{LO}^{(p)} = 48.34\ \text{meV} \qquad \hbar\omega_{LO}^{(c)} = 62.70\ \text{meV}$$

and for O_{18} we have

$$\hbar\omega_{LO}^{(p)} = 45.97\ \text{meV} \qquad \hbar\omega_{LO}^{(c)} = 59.83\ \text{meV}.$$

Making use of these results in equations (30), (31), (7) and (8), our calculations show that

$$\bar{n}_s = 1.37 \times 10^{14}\ \mathrm{cm}^{-2} \qquad n_{1D} = 0.75 \times 10^7\ \mathrm{cm}^{-1} \qquad k_{yF}a = 0.29\ \pi$$

$$k_F a = 0.45\ \pi.$$

In our numerical calculations, we fixed the total number of layers (including the chain planes) to be eight. For this case, the dispersion relation in (24) becomes

$$(A^2 - B^2)\left\{(A^2 - B^2)^2 C^2 - 4(A^2 - B^2)ACDE + 4A^2D^2E^2 - B^2D^2E^2\right\} = 0. \tag{39}$$

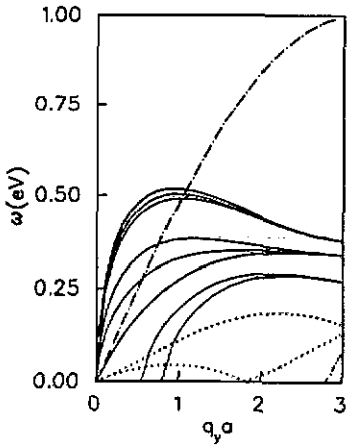

Figure 2. The plasmon energy dispersion for $q_x = 0$, with the phonon coupling set equal to zero. The upper (lower) broken curves represent $\hbar\omega^{(c)}_{max}$ ($\hbar\omega^{(c)}_{min}$). The upper (lower) chain curves are for $\hbar\omega^{(p)}_{max}$ ($\hbar\omega^{(p)}_{min}$). The upper two branches are coupled plane modes and the lowest one is the coupled chain mode.

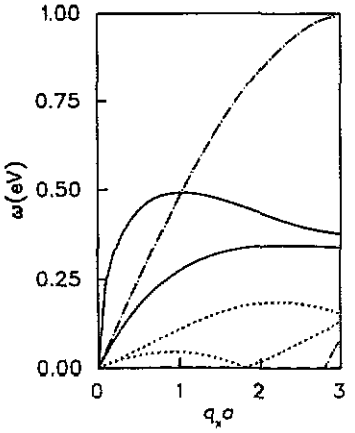

Figure 3. The plasmon energy dispersions for $q_y = 0$ and zero phonon coupling. The notation used in this figure is the same as that in figure 2. Only the coupled plane modes have finite frequency.

Figure 2 shows a plot of the plasmon dispersion relation when $q_x = 0$ and there is no phonon coupling included. Since $W_c \ll W_p$ and $k_{yF} < k_F$, the region where there is Landau damping for the chain is completely contained within the Landau damping region for the plane. As a result of the Pauli exclusion principle, we have $\hbar\omega^{(c)}_{min} \neq 0$ when the magnitude of the wavevector satisfies $q < q_c$. The coupling between layers within a unit cell gives rise to the triple splitting of the spectrum whereas the coupling between the unit cells causes each of these modes, except for the lowest one, to split into three branches. The lowest branch does not split into three branches since there are only two unit cells for the chain planes. The presence of chain planes is responsible for the coupling between the unit cells, leading to the large splitting for the branch in the middle. The highest branch has one local minimum and one maximum at the Brillouin zone boundary and near the centre of

the Brillouin zone, respectively. When $q_y a > 2$, the plasmon modes are localized within one unit cell, causing almost no splitting in this region. The middle branch is the most extended one. When $q_y a$ is small, the coupled chain mode (i.e. the lowest branch) is suppressed due to the narrow bandwidth (or strong localization). Also, since $W_p \gg W_c$, the coupled chain mode is completely Landau damped. The local minimum shifts the plasmon cut-off frequency downward. This effect is not present in a layered homogeneous 2D EG model. If W_p is large, then almost all the plasmon modes will be Landau damped. When W_p is fixed, since the single-particle excitation energy is proportional to W_p, the plasmon energy increases with band filling to reach a maximum at half-filling of the band, i.e. when $k_F a = k_{yF} a = \pi/2$. The calculated maximum plasmon energy is comparable with the observed values in [14]. Our numerical results in figure 2 show that the effect due to the atomic structure can be appreciable when $q_y a > 0.4$.

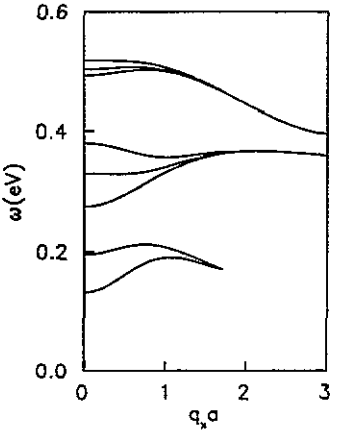

Figure 4. The plasmon energy dispersions for $q_y a = 1.0$ and zero phonon coupling. The upper two branches are coupled plane modes, and the lowest one is the coupled chain mode which is suppressed when $q_x a > 1.75$.

In figure 3, we have plotted the plasmon energy dispersion for $q_y = 0$ in the absence of phonon coupling. Since there are no chain excitations when $q_y = 0$, the coupling between pairs of unit cells is effectively turned off. For this reason, we only get the coupled plane modes which is obtained by solving $A^2 - B^2 = 0$. The triple-splittings arising from the coupling between pairs of unit cells and within a unit cell are set equal to zero. Comparing figure 2 with figure 3, we can see quite clearly the anisotropic dispersion along the q_x and q_y directions, which could be attributed to the inclusion of chain planes in our model calculations. Moreover, from equations (9), (10), (13), (14) and (24), it is not difficult to prove that both the single-particle excitations and the plasmon excitations are periodic along the q_x and q_y directions with the period of the reciprocal lattice vector $G = 2\pi/a$. Contrary to speculation, the chain planes do not increase the weight of acoustical plasmons in the density of states due to the Landau damping from the single-particle excitations in the planes.

Ignoring the phonon coupling, the plasmon energy dispersion for $q_y a = 1.0$ is plotted in figure 4. Here, the chains are excited. However, when $q_x a$ is large the interlayer Coulomb interaction is greatly reduced. This leads to the suppression of the coupled chain modes when $q_x a > 1.75$. Comparing figure 4 with figure 2, we

see that the localization produced by interlayer Coulomb interactions is even stronger when dispersion is along the q_x direction. This also demonstrates that the dispersion is anisotropic in the presence of chain planes. As a result of the periodicity of the lattice, the large splitting between the modes produced by the coupling within the same unit cell can still be maintained at the Brillouin zone boundaries even though the coupling between unit cells has become almost zero. In a straightforward way, we see from (39) that the crystalline structure maintains the dependence of the position of the chain planes on the plasmon energy. When the crystallinity is neglected, i.e. $n = m = 0$ the plasmon excitation energy does not depend on the position of the chains because all the terms involving the product DE in (39) only depend on $2d_1 = d_1' + d_1''$ in this case.

To get an overview of the principal features of the plasmon excitation spectrum, we have plotted the highest branch in 3D in figure 5; the phonon coupling is included in these calculations. We clearly see the four local minima located at the four boundaries of the region in figure 5. Also, the four maxima are situated along the two diagonal lines near the four corners. The region near the centre is quite flat. Furthermore, near the four corners the energy is reduced for a plasmon which is excited along the two diagonal lines.

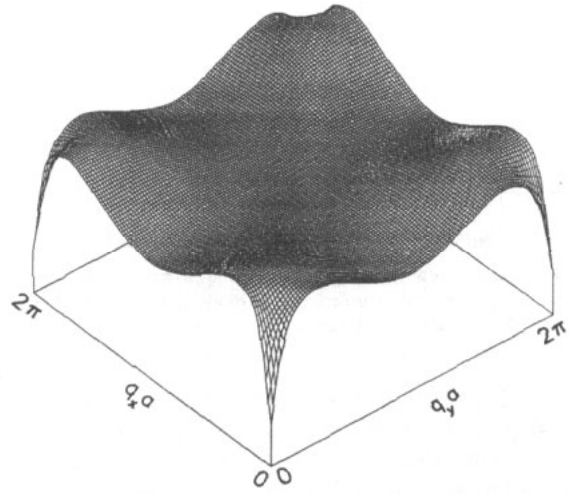

Figure 5. Three-dimensional plot of the plasmon excitation energy spectrum for the highest branch when the O_{16} phonon coupling is included. There are four local minima on the four boundaries. Four maxima near the corners are located along the two diagonal lines. The centre of the displayed region is quite flat. In the vicinity of the four corners, the energy is lower when plasmons are excited along with wavevectors along the two diagonal lines.

In figure 6, we show a plot of the dispersion relation for all the branches of plasmon excitation for $q_x = 0$ when the O_{16} phonon coupling is included. The small optical phonon energies for both the planes and the chains produce the anticrossing in the vicinity of the origin. There are two groups of plasmons due to the splitting produced by the plasmon–phonon coupling. The group with the higher energy are plasmon-like while the lower group are the optical phonon-like modes. The coupling to plasmons leads to weak dispersions for these phonon-like modes. Comparing these

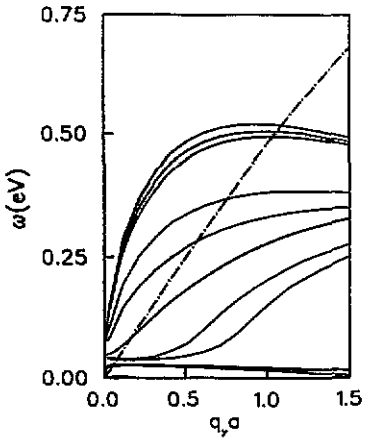

Figure 6. The plasmon energy dispersion relation for $q_x = 0$ when the O_{16} phonon coupling is included. The chain curve represents $\hbar\omega_{max}^{(P)}$ as in figure 2. The anticrossing near the origin is due to plasmon–phonon coupling.

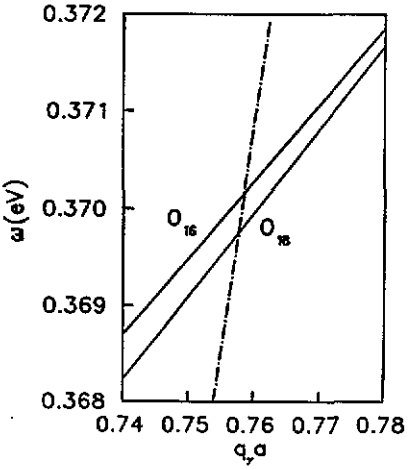

Figure 7. The shift in the plasmon cut-off frequency due to the O_{16}–O_{18} isotope effect for the fourth mode (from the top) in figure 6. Here, $q_x = 0$ and the chain curve has the same meaning as in figure 6.

results with figure 2, we find that the suppression of the chain modes, when $q_y a$ is small, is significantly reduced due to the opening up of another plasmon-coupling channel. The phonon-like modes are well localized on the planes, and the middle branch of the plasmon-like modes is still the most extended one. The chain mode is still completely damped, as in figure 2.

In figures 7 and 8, we have displayed the plasmon cut-off frequency shifts due to the O_{16}–O_{18} isotope effect. Figure 7 shows the shift of the fourth mode (from the top), whereas figure 8 shows the shift in the highest mode. The shift of the highest mode is probably smaller as a result of the localized nature of this mode. The largest indirect shift of the plasmon cut-off frequency is an order of magnitude smaller than the direct shift of the optical phonon frequency. The shift of the chain mode is believed to be larger since the shift of the optical phonon mode for the chain

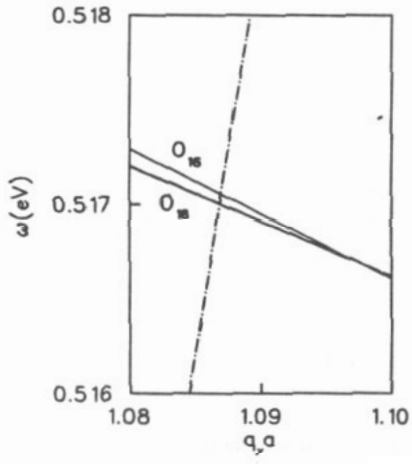

Figure 8. The shift in the plasmon cut-off frequency due to the O_{16}–O_{18} isotope effect for the highest mode in figure 6. Here, $q_x = 0$ and the chain curve has the same meaning as in figure 6. The localized character of this mode reduces the shift.

is larger than it is for the plane and the plasmon-phonon coupling of the chains is stronger than for planes since the plasmon and phonon energies are closer. However, the localized character of the chain mode for small $q_y a$ will significantly limit any increases of the shift in plasmon frequency.

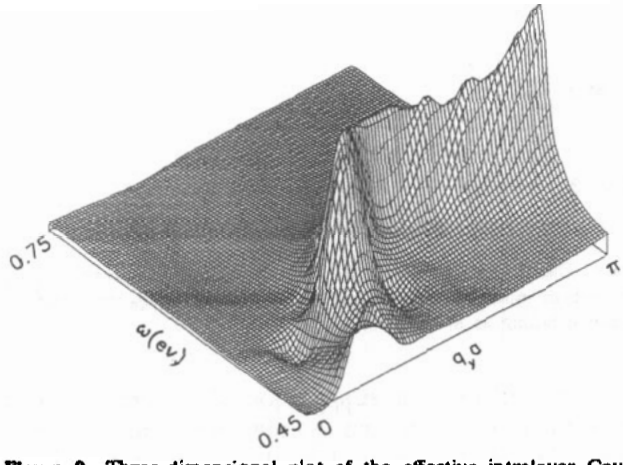

Figure 9. Three-dimensional plot of the effective intralayer Coulomb interaction ratio of (32) in our model to (38) which is a simplified result for a layered 2D EG model as functions of ω and q_y. Here, we take $q_x a = 0.5$ and $q_z d = 1.0$.

In figure 9, we plot the ratio of (32) to (38) as functions of ω and q_y. This function can be taken as a renormalization factor in the gap equation for a layered 2D EG model. The local peaks and valleys in this figure represent the contributions due to plasmons from (32) and (38), respectively. The separation between the positions for the peaks and valleys comes from the combined effects of crystallinity, exchange and correlation, and plasmon–phonon coupling. From (32), we know that the peak

value is proportional to $\epsilon_c/\chi_0^{(p)}$. Since $|\bar{V}|^2$ is usually very small in our model and the optical phonon frequencies for both the chain and plane are almost equal, this gives rise to one plasmon-like and two phonon-like modes whose energies are nearly equal to the energies of the single chain plane plasmon-like or phonon-like modes, which corresponds to the solutions of $\epsilon_c = 0$. The remaining plasmon-like modes with energies close to the energy of a single-plane plasmon mode correspond to solutions of $\epsilon_p = 0$ in the absence of phonon coupling. Therefore, only one dominant peak in figure 9 is conspicuously seen. If the coupling term $|\bar{V}|^2$ is sufficiently strong, we believe we would see the other three smaller peaks. A similar situation can be seen in figure 10, where we have plotted the ratio of (32) to (38) as functions of ω and q_z. Here, we also get one valley and one dominant peak. By tracing the peak, we obtain the q_z-dependence of the plasmon excitation energy. In both figures 9 and 10, we have found that the ratio has a value larger than one in most regions of the figures. This implies that the chains increase the magnitude of the effective intralayer Coulomb interaction. Equation (33) implies that the corrections due to exchange and correlation reduce the short-ranged part of the Coulomb interaction, and this usually leads to a reduction of the plasmon excitation energy.

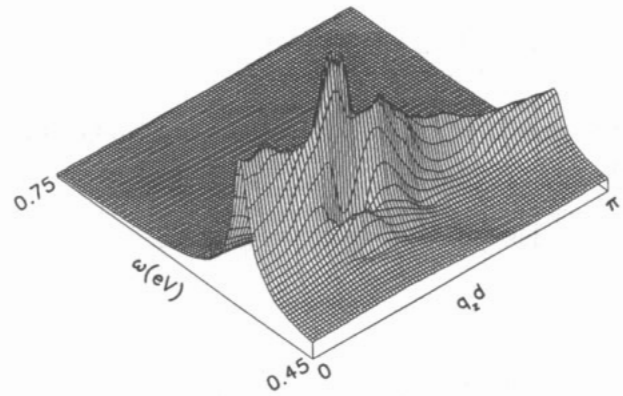

Figure 10. Three-dimensional plot of the effective intralayer Coulomb interaction ratio of (32) in our model to (38) which is a simplified result for a layered 2D EG model as functions of ω and q_z. Here, we take $q_x a = q_y a = 1.0$.

Our calculations also show that increasing the number of planes within a unit cell will greatly increase the plasmon energy as well as the weight of acoustical plasmons in the density of states due to the very strong interlayer coupling within a unit cell. We emphasize that the role of chain planes is to increase the coupling between the unit cells.

4. Discussion

In this section, we expand the previous discussion to establish a connection between our results and the experimental data for high-T_c superconductors. From a linearized version of the Eliashberg equation in conjunction with some simplifying approximations [6,15,16] we obtain the transition temperature for s-wave pairing when $\omega_c \ll \epsilon_F^{(p)}$

as

$$k_B T_c = 1.134 \hbar \omega_c \exp\left\{-\left(\frac{\lambda+1}{\lambda-\mu^*}\right)\right\} \tag{40}$$

where μ^* is the modified Coulomb repulsive potential, defined by

$$\mu^* = \frac{\mu}{1+\mu \ln\left(\epsilon_F^{(p)}/\hbar\omega_c\right)}. \tag{41}$$

Here, the Fermi energy $\epsilon_F^{(p)}$ is given by (16), ω_c is a plasmon cut-off frequency and μ is an averaged screened Coulomb repulsion, defined by

$$\mu = \frac{d}{2\pi}\int_{-\pi/a}^{\pi/a} dq_z \frac{N_{2D}\left(\epsilon_F^{(p)}\right)}{4k_F^2}\int_0^{2k_F} dq_x \int_0^{2k_F} dq_y U_{\text{eff}}(q;\omega=0) \tag{42}$$

where d is the length of the unit cell. k_F and U_{eff} are defined in (8) and (32), respectively, and

$$N_{2D}\left(\epsilon_F^{(p)}\right) = \frac{1}{\pi W_p a^2}\left[\frac{k_F a}{\sin(k_F a)}\right] \tag{43}$$

is the 2D single-particle density of states at the Fermi energy. λ in (40) is an attractive potential defined by

$$\lambda = 2\int_0^{\omega_c} d\omega \frac{\alpha^2(\omega)F(\omega)}{\omega} \tag{44}$$

where

$$\alpha^2(\omega) = \frac{d}{2\pi}\int_{-\pi/d}^{\pi/d} dq_z \frac{N_{2D}\left(\epsilon_F^{(p)}\right)}{4k_F^2}\int_0^{2k_F} dq_x \int_0^{2k_F} dq_y U_{\text{eff}}^2(q;\omega) \tag{45}$$

and

$$F(\omega) = \frac{1}{4\pi\hbar}\left[\left|\frac{\partial q_x^2}{\partial\omega_p}\right|_{q_y=q_z=0} + \left|\frac{\partial q_y^2}{\partial\omega_p}\right|_{q_x=q_z=0}\right] + \frac{1}{2\pi\hbar}\left|\frac{\partial q_z}{\partial\omega_p}\right|_{q_x=q_y=0} \tag{46}$$

is the plasmon density of states. $\omega_p = \omega_p(q)$ in (46) is determined as a root of $\epsilon(q;\omega) = 0$ where ϵ is defined in (35). The anisotropy in the density of states is again quite clear from (46). This is due to the two-dimensionality and the inclusion of chain planes into our model. Furthermore, when $q_z a = \pm\pi$, $|\partial q_z/\partial\omega_p|$ in the density of states becomes singular and makes the dominant contribution to the weight of acoustical plasmons.

Clearly, from (40), T_c increases with ω_c or λ. The chain planes in our model increase the coupling within a unit cell as well as the effective intralayer Coulomb interaction. As a result, ω_c and λ are enhanced in magnitude which in turn causes the superconducting transition temperature to increase.

Assuming a plasmon-mediated pairing mechanism, we can calculate the isotope effect through the index β defined in terms of the following logarithmic derivative

$$\beta = -\frac{d \ln (\omega_c)}{d \ln (M_0)} \tag{47}$$

that in olves the mass M_0 of the oxygen atom. In our numerical calculations, $\omega_c \sim (0.4 - 0.5)$ eV, but $\epsilon_F^{(p)} = 4.2$ eV. This implies that the condition $\omega_c \ll \epsilon_F^{(p)}$ for equatic ns (40) and (41) is well satisfied. The isotope effect also influences the values of λ ar l μ^* as a result of changes in U_{eff} and $F(\omega)$. In our numerical calculations, we have f nd that these changes are small. Therefore, we have neglected the resulting small r odifications in λ and μ in (47). Referring to figure 7, we deduce the cut-off freque cies for O_{16} and O_{18}. These yield $\beta = 0.58 \times 10^{-2}$ which is two orders of magnit de smaller than the standard BCS value of 0.5. It was argued in [15] that the pair-br aking effect would lower β by one order of magnitude. The smaller value of β that ve obtain is due to the fact that no direct phonon-mediated pairing process is involve l.

In onclusion, we emphasize that the local minimum in the excitation energy spectru n is due to the crystalline structure within the layers of the superlattice. We have sl own that the plasmon–optical phonon coupling produces a shift in the plasmon cut-off requency. We have also demonstrated that incorporating the chain planes into our mc lel increases the coupling between unit cells as well as the intralayer Coulomb interac ion which in turn produces a higher T_c.

Ackno ledgments

We wc uld like to thank Dr M Mohamed for helpful discussions. This work was suppor ed in part by a grant from the Natural Sciences and Engineering Research Counc of Canada (DH and GG).

Refere ces

[1] A derson P W 1987 *Science* **235** 1196
A derson P W, Baskaran G, Zou Z and Hsu T 1987 *Phys. Rev. Lett.* **58** 2790
K elson S A, Rokksar D S and Sethna J P 1987 *Phys. Rev.* B **35** 8865
[2] L ghlin R B 1988 *Phys. Rev. Lett.* **60** 2677
[3] S rieffer J R, Wen X G and Zhang S C 1988 *Phys. Rev. Lett.* **60** 944
[4] B deen J, Cooper L N and Schrieffer J R 1957 *Phys. Rev.* **108** 1175
[5] M rris D E, Kuroda R M, Markelz A G, Nickel J H and Wei J Y T 1988 *Phys. Rev.* B **37** 5936
[6] R alds J 1987 *Phys. Rev.* B **35** 8869
[7] K sin V Z and Morawitz H 1988 *Phys. Rev.* B **37** 7854
[8] G ffin A 1988 *Phys. Rev.* **37** 5943
[9] G ffin A and Pindor A J 1989 *Phys. Rev.* B **39** 11503
[10] T y S F, Wang S Y and Yang T J W 1990 *Phys. Lett.* A **151** 439
[11] H ang D and Antoniewcz P R 1991 *Phys. Rev.* B **43** 2169
H ang D and Zhou X 1990 *J. Phys.: Condens. Matter* **2** 501
[12] T gman S A 1990 *Phys. Rev. Lett.* **65** 500
[13] F nk J P, Jung J, Salomons G, Miner W A, Mohamed M A -K, Chrznowski J, Gygax S, Irwin J C, Mitchell D E and Sproule G I 1990 *Physica* C **172** 90
[14] P kowitz S, Carr G L, Lou B, Yom S S, Sudharsann R and Ginley D S 1987 *Solid State Commun.* **64** 721

Krenn H, Bauer G, Vogl G, Strässer G and Gornik E 1989 *Phys. Rev.* B **39** 6716
Cooper J R, Chu C T, Zhou L W, Dunn B and Gruner G 1988 *Phys. Rev.* B **37** 638
Genzel L, Wittlin A, Kuhl J, Mattausch H, Bauhofer W and Simon A 1987 *Solid State Commun.* **63** 843
[15] Carbotte J P, Greeson M and Gonzalez A P 1991 *Phys. Rev. Lett.* **66** 1789
[16] Gumbs G 1983 *J. Low Temp. Phys.* **50** 85